Estrogen Receptor Beta Activation Coordinates Liver Lipid Remodeling and Metabolic Fluxes, Preventing Lipotoxicity

Debora Santos Rocha*[1,2], Eloisa Vilas-Boas[3], Camille C. Caldeira da Silva[1,2], Everton L. Vogt[1,2], Marcos Yoshinaga[4], Mariana Pacheco Teixeira de Carvalho[1,2], Maiara I. C. Queiroz[1,2], Tiago Eugênio Oliveira da Silva[1,2], Sayuri Miyamoto[1,2], Alicia J. Kowaltowski[1,2]

[1] Departamento de Bioquímica, Instituto de Química, Universidade de São Paulo, São Paulo, Brazil

[2] Centro de Metabolismo CoMeta, Hospital Universitário, Universidade de São Paulo, São Paulo, Brazil

[3] Departamento de Análises Clínicas e Toxicológicas, Faculdade de Ciências Farmacêuticas, Universidade de São Paulo, São Paulo, Brazil

[4] PinguisLab, Universidade Cruzeiro do Sul, São Paulo, Brazil

*Corresponding author:

Debora Santos Rocha

Av. Prof. Lineu Prestes, 748, São Paulo, Brazil

+551130918556

debora.santosrocha@usp.br

ABSTRACT

Non-selective hormone replacement with estradiol is known to improve metabolic homeostasis during menopause. However, this treatment is not recommended for individuals with genetic predisposition to hormone-responsive cancers. In contrast, selective activation of estrogen receptor beta (ERβ) has shown promising results, promoting antitumor effects and modulating metabolic outcomes, although the mechanisms in which these changes occur remain poorly understood. We investigated the effects of ERβ activation using diarylpropionitrile (DPN), a selective ERβ agonist, in both an *in vivo* model of post menopause and *in vitro* model of metabolic overload. Female Wistar rats were submitted to ovariectomy (OVX) and later treated with DPN. ERβ agonist treatment recovered fasting glucose and lipid profiles, improved pancreatic islet morphology, and reduced retroperitoneal white adipose tissue. Serum ketone bodies and free fatty acid levels were also recovered to control levels, suggesting modulation in liver lipid oxidation. DPN treatment also promoted substantial lipidome remodeling specifically in OVX animals, generating a lipid-buffering profile. To isolate the effects mechanistically, hepatocytes were submitted to nutrient overload and treated with DPN. *In vitro*, DPN also recovered ketone body secretion and promoted an increased dependence on complete fatty acid oxidation, as well as decreased metabolic flexibility, as assessed by modulated extracellular flux analysis. Overall, these findings demonstrate a new role of ERβ in the modulation of hepatic lipid and ketone metabolism, with positive metabolic outcomes in estradiol-deficient animals.

Keywords: estradiol receptor beta; mitochondria; lipidomics; menopause; MASLD

ABBREVIATIONS

AC, acylcarnitine; AML-12, alpha mouse liver 12 cells; BSA, bovine serum albumin; BW, body weight; CCCP, carbonyl cyanide m-chlorophenyl hydrazone; CE, cholesteryl esters; CPT2, carnitine palmitoyltransferase 2; DMEM, Dulbecco's modified Eagle's minimal essential medium; DPN, diarylpropionitrile; ER, estrogen receptor; ERα, estrogen receptor alpha; ERβ, estrogen receptor beta; ERβ, estrogen receptor beta; ETFA, electron transfer flavoprotein subunit alpha; FA, fatty acid; FBS, fetal bovine serum; FC, free cholesterol; FFA, free fatty acid; GPER, G protein-coupled estrogen receptor; GTT, glucose tolerance test; HDL, high-density lipoprotein; HGP, high glucose-palmitate; HRT, hormone replacement therapy; LD, lipid droplet; LDL, low-density lipoprotein; LGB, low glucose-BSA; MTBE, methyl-tert-butyl ether; NEFA, non-esterified free fatty acid; OCR, oxygen consumption rate; OVX, ovariectomy; PCA, principal component analysis; PDH, pyruvate dehydrogenase; PKA, protein kinase A; PKC, protein kinase C; TG, triglycerides; Tim23, translocase of the inner mitochondrial membrane 23; VLDL, very low-density lipoprotein; WAT, white adipose tissue; WATr, retroperitoneal white adipose tissue.

41 ## 1. INTRODUCTION

42 Estrogen signaling plays a central role not only in reproductive functions, but also
43 in energy metabolism, stimulating insulin production and secretion in pancreatic beta
44 cells, and improving peripheral insulin signaling in the adipose tissue, muscle, and liver
45 (1,2). Accordingly, postmenopausal decreases in estradiol levels lead to various
46 metabolic consequences, including increased risk of metabolic disease development.
47 This is observed both in humans and in animal models of estrogen deficiency induced
48 by ovariectomy or hypothalamic-pituitary-gonad axis modulation (3). Estrogen
49 deficiency also promotes the accumulation of visceral white adipose tissue and
50 circulating free fatty acid (FFA) overload (4,5). Chronically increased FFA levels
51 compromise postprandial muscle glucose uptake and promote decompensation of
52 hepatic glucose production. Consequent long-term glucotoxicity and lipotoxicity affect
53 endocrine pancreatic responses to energy demands, culminating in defective insulin
54 production and secretion, worsening the already impaired peripheral tissue insulin
55 sensitivity (6,7).

56 In this sense, it is reasonable to assume that hormone replacement therapy
57 (HRT) with estradiol would promote metabolic benefits postmenopause. In fact, HRT
58 modulates adipose tissue redistribution to an insulin-sensitive phenotype, increasing
59 subcutaneous and decreasing visceral depots (8), in addition to attenuating the
60 metabolic imbalance associated with type II diabetes mellitus (9,10). However, non-
61 selective activation of estradiol receptors (ERs) often provides only transient benefits
62 which wane over time, and displays risks such as increased incidence of hormone-
63 responsive tumor development in patients with gynecological cancer predisposition
64 (11,12).

65 Estradiol used in HRT activates the 3 main types of estrogen receptors: nuclear
66 receptors alpha (ERα) and beta (ERβ) as well as membrane receptors (GPER). ERα and
67 ERβ trigger estrogen response element binding, modifying gene transcription and,
68 consequently, protein synthesis. These genomic responses to estrogens occur within
69 hours. Conversely, the activation of GPER leads to a rapid response, within seconds or

70 minutes, modulating cytosolic signaling processes including calcium influx (13) and
71 activation of PKA and PKC pathways (14).

72 Selective ERα activation attenuates energy imbalance, improves insulin
73 sensitivity, changes white adipose tissue (WAT) phenotypes and promotes browning
74 (2,15,16). The outcomes of selective ERβ activation results are still poorly characterized,
75 although data also suggest changes in WAT storage patterns, shifting from visceral to
76 subcutaneous predominance (15), as well as WAT browning, and increased insulin
77 sensitivity signs (17) as evidenced by enhanced glucose uptake in muscle fibers (18).
78 These effects remain to be characterized mechanistically.

79 In the liver, estradiol reduces the imbalanced accumulation of triacylglycerol,
80 and consequently steatosis, while also reducing gluconeogenesis, results that are
81 generally attributed to ERα activation due to its relative high expression levels (19–21).
82 The selective activation of ERβ in female rodents is also capable of triggering responses
83 in hepatocytes, reducing adipogenesis and lipid accumulation (22). If these effects are
84 also observed under postmenopausal conditions remains to be explored.

85 Determining if selective ERβ activation promotes metabolic changes
86 postmenopause is of interest because, while ERα activation is associated with the
87 development of hormone-dependent cancers (23), ERβ activation has antitumor (24–
88 26), cell cycle inhibitory (27), and antiangiogenic effects (23,28). It is thus reasonable to
89 assume that selective modulation of ERβ would be a promising alternative therapeutic
90 strategy for postmenopausal metabolic syndrome. Therefore, the aim of this paper is to
91 describe the metabolic effects of selective beta estradiol receptor (ERβ) activation under
92 postmenopausal conditions, with a focus on the liver as a central metabolic hub.

93

94 ## 2. MATERIALS AND METHODS

95 ### 2.1. Animals

96 Female Wistar rats (n = 5-7 per group, total = 26) were randomized, acclimatized for
97 20 days, and maintained at controlled temperatures (23°C) with 12-12 h light/dark cycles
98 and *ad libitum* access to food/water. A pilot and an experimental study (including all

experimental groups) were conducted. All procedures were conducted in accordance with the Ethical Principles of Animal Manipulation of the local animal ethics committee (CEUA-IQ/USP protocol 244/2022), the National Research Council Guide for the Care and Use of Laboratory Animals, and follow ARRIVE Guidelines (29–31).

At 90 days of age, animals were submitted to ovariectomy as described in the "Ovariectomy surgery" section. Fifteen days later, they began treatment with ERβ agonist diarylpropionitrile (DPN, 1 mg · kg^{-1} · day^{-1}, s.c.) or vehicle (sesame oil) for 15 days. Four groups were studied: sham surgery treated with vehicle (Vehicle); sham surgery treated with DPN (DPN); ovariectomized animals treated with vehicle (OVX vehicle); and ovariectomized animals treated with DPN (OVX DPN). The animals were observed for 30 days for their food intake, weight gain, and glucose tolerance (described under "Glucose tolerance test"). At the endpoint, animals were anesthetized and killed by cardiac punction. Serum was obtained after total blood centrifugation (20 minutes at 300 g) and stored for further analysis. Retroperitoneal white adipose tissue (WATr), uteruses, and livers were collected and weighed. WATr, pancreases, and livers were evaluated for histological characteristics (see "Histology analysis"). The liver was also used for mitochondrial isolation; fresh mitochondria were used to measure oxygen consumption rates as described in the "Oxygen consumption assay" section.

2.2. Ovariectomy surgeries

90-day-old female Wistar rats were anesthetized (4% isoflurane for induction and 1.5% for maintenance) and monitored for temperature, heartbeats, and ventilation rates. Rats were positioned in ventral decubitus, and an incision was made between the lower costal margin and thigh, approximately 1 cm from the midline. The muscle wall was retracted, then the ovary was located within the adipose tissue and removed after ligation of the corresponding uterine tube by sectioning between the ligature and the ovary. Muscle and skin were then sutured, and the procedure was repeated on the contralateral side (32). After surgery, the animals were monitored and treated with tramadol (20 mg/kg) for analgesia. None of the animals presented pain or distress considering the Grimace scale (33) Sham surgery animals also underwent the same procedures, except for the removal of the ovaries.

129

130 ## 2.3. Glucose tolerance tests

131 Glucose tolerance was evaluated before the ovariectomy surgery (week 1); 15 days
132 after surgery and before DPN treatment (week 3); and after 30 days of surgery and 15
133 days of DPN treatment (week 5). The animals were submitted to 6 hours of food
134 deprivation and basal glucose levels were registered. Glucose (1 g per kg of body weight)
135 was diluted in isotonic saline solution (NaCl 0.9%) and injected intraperitoneally. Blood
136 glucose levels were registered at 5, 15, 30, 60, 90, and 120 minutes using a Roche Accu-
137 Chek glucometer.

138 ## 2.4. Histological analysis

139 WATr, pancreas, and liver tissues were fixed in buffered formalin, dehydrated with
140 ethanol solutions (70 to 100 %), embedded in paraffin, sectioned, mounted on slides,
141 deparaffinized, and stained with hematoxylin/eosin. Images were registered with an
142 Axio Scan.Z1 slide scanner and analyzed using QuPath software.

143 Pancreases were evaluated for islet morphometric parameters. The endocrine tissue
144 was visually identified, and islets were circulated individually. The shape descriptor tool
145 was used to measure size and circularity. Islets were divided into quartiles as small,
146 medium, or large using the control group as a reference (34–36).

147 WATr was analyzed according to Palomäki *et al.* (37). The software was trained using
148 the "train pixel classifier" tool. The brush and expected size range were used as training
149 inputs. The "create objects" tool was then used and cell-by-cell visual confirmation
150 ensured correct output compared to the original image. The "shape descriptors" tool
151 was used to analyze average adipocyte areas (μm^2).

152 Liver histology was evaluated for macrovesicular steatosis, considering the non-
153 stained area within the tissue (apart from the portal vein branch area). Positive areas
154 for macrovesicular steatosis were described as percentage of total area and interpreted
155 as neutral lipid accumulation *in vivo* (38,39).

156 ## 2.5. Biochemical serum analysis

157 Serum total cholesterol, HDL, LDL, triglycerides, free fatty acids, and beta
158 hydroxybutyrate were detected using commercial kits (LabTest®, FUJIFILM®, and Sigma
159 Aldrich®). VLDL levels were calculated by subtracting the measured HDL and LDL
160 cholesterol fractions from total cholesterol. Sample preparation, dilution, and standard
161 curve protocols were conducted according to manufacturer instructions.

162 ## 2.6. Tissue glycogen and triglycerides

163 Samples were hydrolyzed with 30% KOH at 100°C. Glycogen was precipitated in 70%
164 ethanol, washed with distilled water, and converted into glucose by adding 4 M HCl at
165 100°C. Glycogen levels were measured based on glucose quantities resulting from
166 hydrolysis compared to a commercial standard glycogen sample (Sigma-Aldrich)
167 previously hydrolyzed in HCl. Detection was performed using a commercial glucose
168 assay kit (LabTest®). Triacylglycerol was detected using a commercial kit (LabTest®). Data
169 were expressed as µg triglycerides per µg protein and mg glycogen per mg tissue.

170 ## 2.7. Lipidomics

171 Liver samples (approximately 200 mg) were homogenized in PBS buffer containing
172 20 µM deferoxamine and subjected to methyl-tert-butyl ether (MTBE) extraction (40).
173 Lipid extracts were analyzed via an untargeted lipidomics approach using ultra-high-
174 performance liquid chromatography (UHPLC; Nexera, Shimadzu, Kyoto, Japan) coupled
175 with electrospray ionization tandem time-of-flight mass spectrometry (ESI-MS/MS)
176 (Triple TOF® 6600, Sciex, Concord, USA). Lipid species were identified by inspecting
177 MS/MS spectra using PeakView® (Sciex). Each lipid molecular species was quantified by
178 normalizing the precursor ion peak area to that of the corresponding internal standard
179 using MultiQuant® (Sciex). Concentrations were calculated based on the ratio of
180 integrated MS data to the sample volume, and results were expressed as a percentage
181 of total lipids or in nmols per mg of protein. The coefficient of variation (CV) was
182 calculated to filter lipid species displaying CV>20%, based on 5 quality control samples
183 measured during the experimental routines in ESI-MS/MS. Data was log10-transformed
184 to achieve normal distribution. One-way ANOVA followed by FDR correction (196
185 altered compounds, $p<0.05$) was used to compare the amount of lipids changed
186 between four experimental groups. A heatmap displaying the top 75 lipid species

187 (lowest ANOVA p-values) were built using Euclidean distance and Ward clustering. The
188 top 75 lipid species (lowest ANOVA p-values) are displayed. For Principal Component
189 Analysis (PCA) analysis, normalized (log10-transformed) data were visualized in a 2D PCA
190 plot showing PC1 and PC2 (X% and Y% of variance, respectively). For cholesteryl esters
191 (CE) and triglycerides (TG), only CE and TG associated lipids with statistically significant
192 differences (t-test, two-group comparison; $p<0.05$) were analyzed; fold-change was
193 then calculated for each significantly altered feature. All statistical analysis were
194 performed in MetaboAnalyst (https://www.metaboanalyst.ca/,(41)). For TG fatty acid
195 (FA) analysis, the molar abundance of each individual fatty acid (FA) within TG species
196 was calculated and normalized to the total TG molar concentration for t-test and fold-
197 change analyses. TG were further categorized by FA saturation status as: saturated (S),
198 monounsaturated (M), polyunsaturated (P, 2-3 double bonds), and highly unsaturated
199 (H, >3 double bonds).

200 ## 2.8. Mitochondrial oxygen consumption measurements

201 The liver was chopped, suspended in isolation buffer (250 mM sucrose, 10 mM
202 HEPES, 1 mM EGTA, 1 mM EDTA, 1 mg/mL BSA, pH 7.2, at 4°C), and manually
203 homogenized using a Potter–Elvehjem tissue grinder. The suspension was centrifuged
204 twice (800 g, 4°C, 4 min), and the pellet discharged. The supernatant was further
205 centrifuged at 9000 g, 4°C for 10 min. The pellet was resuspended in resuspension buffer
206 (300 mM sucrose, 10 mM HEPES, and 2 mM EGTA, pH 7.2) and centrifuged again (12000
207 g, 4°C, 10 min). The pellet was resuspended in 1 mL resuspension buffer, and total
208 protein was quantified using the Bradford method.

209 For respirometry assays, 250 µg or 50 µg protein (for CI or CII–linked respiration,
210 respectively) of isolated mitochondria were incubated in a buffer containing 120 mM
211 sucrose, 65 mM KCl, 2 mM $MgCl_2$, 1 mM KH_2PO_4, 1 mM EGTA, 10 mM HEPES, and 0.1%
212 fatty acid-free BSA, pH 7.2, at 37°C in an Oroboros O2k high-resolution respirometer
213 (Innsbruck, Austria). 1 mM pyruvate plus 1 mM malate and 1 mM α-KG, or 1 mM
214 succinate plus 1 µM rotenone were used to induce CI-linked and CII-linked oxygen
215 consumption, respectively. Oxygen consumption was monitored through sequential

216 additions of ADP (1 mM) to induce state 3, oligomycin (1 µM) to induce state 4, and
217 CCCP (titrated in 100 nM additions) for state 3u, as described in previous studies (42).

218 ## 2.9. Cell cultures

219 Non-tumor alpha mouse liver 12 cells (AML12, ATCC® CRL-2254™) were cultivated
220 in Dubelco's modified Eagle's minimal essential medium (DMEM, GIBCO®, Life
221 Technologies) - low glucose (5.6 mM) - supplemented with 10% fetal bovine serum (FBS)
222 and 1% antibiotic-antifungal solution (Microlab®), 1.7 µM Insulin, 0.069 µM Transferrin,
223 0.038 Sodium Selenite, without Phenol Red. The cells were kept in a humidified
224 incubator at 37°C, in an atmosphere of 5% CO_2 and 95% air.

225 Cells were plated and, after 24 hours (~80% confluence), the medium was replaced
226 with treatment medium lacking FBS. Experimental groups were as follows: low glucose-
227 BSA (LGB), high glucose-palmitate (HGP), and HGP plus ERβ agonist (DPN at 0.1 nM or 1
228 nM for an additional 24 h). The LGB group received BSA (0.25%) plus low glucose (5.6
229 mM). The HGP group was exposed to BSA-Palmitate (200 µM) plus high glucose (20
230 mM).

231 ## 2.10. Fluorescence microscopies

232 24 h after treatment, mitochondrial morphology was verified in cell cultures through
233 live 3D fluorescence microscopy. Cells were loaded with Mitotracker Deep Red (50 nM)
234 and BODIPY (1 µM) for 20 minutes. The media was then replaced by PBS, and images of
235 live cells were taken using a Leica DMi8 fluorescence microscope (43). The mitochondrial
236 network was analyzed using the Mitochondrial Analyzer plugin (ImageJ software) and
237 evaluated for mean volume and sphericity. Lipid droplets were assessed for their count
238 and area per cell. 40 to 50 cells were quantified per group for each biological replicate.
239 At least 5 different captured images were analyzed per biological replicate (n = 5).

240 ## 2.11. Mitostress tests

241 After treatment, cells were washed in PBS twice and incubated in DMEM containing
242 5.6 mM glucose, 1% penicillin/streptomycin, and 5 mM HEPES, without FBS or
243 bicarbonate. Oxygen consumption rates (OCRs) were quantified using an extracellular

244 flux analyzer (Seahorse XF24). Basal respiration was registered, and mitochondrial
245 modulators were injected sequentially to quantify ATP-linked, maximal, and non-
246 mitochondrial respiration by injecting oligomycin (1 µM), CCCP (1 µM), and antimycin
247 plus rotenone (1 µM each), respectively. All mitochondrial modulators were titrated
248 separately in preliminary experiments under LGB and HGP conditions (due to the
249 possible quenching effect of fatty acids), and doses used were the minimal required for
250 a maximal response (42).

251 ## 2.12. Metabolic flexibility assays

252 After treatment, cells were washed in PBS twice and incubated in DMEM containing
253 5.6 mM glucose, 1% penicillin/streptomycin, and 5 mM HEPES, without FBS or
254 bicarbonate. OCRs were quantified using a Seahorse XF24 extracellular flux analyzer. In
255 the metabolic flexibility assay, cells were sequentially submitted to specific oxidation
256 pathway inhibitors: Etomoxir (CPT1/FFA oxidation inhibitor - 7 µM), BPTES
257 (glutaminase/GSL1 inhibitor - 8 µM), and UK5099 (mitochondrial pyruvate transporter
258 inhibitor - 6 µM). A decrease in OCR after the inhibitor injection indicates the
259 dependence on the specific substrate (when only this pathway is inhibited), and the
260 maximum capacity to oxidize the specific substrate is obtained when the alternative
261 pathways are inhibited. Metabolic flexibility was calculated as the difference between
262 dependence and capacity, indicating cell effectiveness in changing substrate use. All
263 concentrations used were previously titrated under LGB and HGP conditions, as
264 described above.

265 ## 2.13. Western blots

266 Cells were homogenized in RIPA buffer containing 50 mM HEPES, 40 mM NaCl, 50
267 mM NaF, 2 mM EDTA, 10 mM sodium pyrophosphate, 10 mM sodium glycerophosphate,
268 2 mM sodium orthovanadate, 1% Triton-X 100, and protease inhibitors without EDTA,
269 then centrifuged at 13,000 rpm for 10 minutes at 4°C. Lysates were diluted in Laemmli
270 buffer, and proteins were separated using a 10% denaturing polyacrylamide gel.
271 Proteins were transferred to nitrocellulose membranes and incubated with specific
272 antibodies (**Table 1**). Secondary antibodies were added for visualization of bands, which
273 were semi-quantified using densitometric analysis with Image J.

2.14. Statistical analysis

Data were evaluated in Prism Graphpad software, using ANOVA and Tukey posttests when data presented gaussian distribution and variance homogeneity, or correlate tests for non-gaussian distributions. For animal data, two-way (OVX and DPN variables) unpaired tests were used to compare different individuals, while repeated measures were applied to compare the same individual over time. The biological replicates necessary were based on the minimum sample size reported in prior studies assessing ovariectomy and subsequent biochemical analyses, ensuring statistical reliability of the results with minimal animal use (32,34,35,37). For *in vitro* data, one-way paired tests were conducted, since each biological replicate was divided across all experimental conditions. Also, unpaired data are displayed as individual dots, and paired analyses are plotted as continuous lines connecting individual experiments. All groups were verified statistically for outliers to be considered in the analysis. Significance was considered for differences where the p value was lower than 0.05.

3. RESULTS

3.1. ERβ agonist DPN modulates glucose homeostasis in ovariectomized (OVX) animals

The *in vivo* metabolic effects of OVX were monitored in female rats over the course of five weeks. Week 1 data were collected under baseline conditions, before the intervention protocol began, just prior to surgeries (OVX or sham). ERβ agonist (DPN) treatment began 15 days later, at Week 3. The experimental design is shown in **Figure 1A**. Measurements included body weight (BW), serum glucose levels, and glucose tolerance tests (GTT) repeated in Week 3 (15 days after OVX surgery, just prior to DPN treatment) and Week 5 (30 days after surgery and at 15 days of DPN treatment), when animals were euthanized and tissue analysis was conducted.

Figure 1B shows that OVX decreases endpoint uterus weights, as expected, with no noticeable effect of DPN. Also, in control animals the estrous cycling was not altered during DPN treatment (**Supplementary material Figure S1**). Weight gain over time

303 (**Figure 1C**) was observed in all groups, and was significantly higher in OVX groups, as
304 expected, with no significant effect of DPN. OVX slightly increased weight gain per
305 calorie ingested, also with no effect of DPN (**Figure 1D**).

306 Glucose tolerance test (GTT) profiles before treatments at Week 1 (**Figure 1E**,
307 area under the curve, and **Figure 1I**, basal glucose) were similar for all groups, indicating
308 appropriate individual distribution prior to interventions. At Week 3 and 5, GTT response
309 remained unchanged (**Figure 1F and 1G**), although basal glucose levels were increased
310 15 days after OVX (**Figure 1J**) and remained significantly elevated in OVX animals relative
311 to controls at Week 5 (**Figure 1K**). DPN promoted an increase in basal glucose levels in
312 control animals, but significantly decreased the elevated basal glucose levels observed
313 in OVX rats, reverting them to control levels. This indicates the ERβ agonist promotes
314 significant glycemic modulation in OVX animals.

315 Given these effects on glucose homeostasis, we also examined endocrine
316 pancreas histology (**Figure 1H**). OVX promoted an increase in smaller islets (**Figure 1L**)
317 and a decrease in islet circularity (**Figure 1M**). DPN specifically increased islet size in the
318 absence of OVX (**Figure 1L**), while partially protecting against the decrease in circularity
319 promoted by OVX (**Figure 1M**).

320 ### 3.2. ERβ activation improves lipid homeostasis in OVX animals

321 Retroperitoneal white adipose tissue (WATr) was also evaluated in response to
322 OVX and DPN (**Figure 2A**), given its importance as a metabolic hub. As expected, OVX
323 animals had a significant increase in WATr tissue weight, an effect that was abrogated
324 by DPN treatment (**Figure 2B**). Interestingly, DPN also decreased average adipocyte
325 areas in both control and OVX animals (**Figure 2C**).

326 In line with these anatomical findings, the serum lipid profile changed
327 remarkably after OVX. Total cholesterol (**Figure 2D**), LDL (**Figure 2F**), and VLDL (**Figure**
328 **2G**), but not HDL (**Figure 2E**), were increased by OVX, with strong protective effects of
329 DPN on total (**Figure 2D**) and VLDL (**Figure 2G**) cholesterol levels. Serum triglycerides
330 were also increased in OVX animals, in a manner prevented by DPN (**Figure 2H**). Serum
331 non-esterified free fatty acid (NEFA) concentrations increased in OVX (**Figure 2I**), an
332 effect accompanied by increased ketone bodies (**Figure 2J**). DPN treatment restored

333 these parameters in OVX animals to control levels (**Figures 2I** and **2J**). Overall, these
334 results indicate that ERβ activation has protective effects against OVX-induced
335 dyslipidemia and also promotes changes in lipid metabolism in the liver, from where
336 ketone bodies are derived.

337 ### 3.3. Post-OVX liver metabolism is modulated by selective ERβ activation

338 Due to its central function coordinating carbohydrate and lipid metabolism,
339 along with the observed evidence of changes in liver-derived ketone bodies, hepatic
340 tissue was evaluated in more detail. Histological (**Figure 3A**) and content analysis
341 showed increased glycogen in OVX animals, an effect reversed by DPN (**Figure 3B**).
342 Surprisingly, DPN had the opposite effect in non-OVX rats, increasing glycogen content
343 in control animals (**Figure 3B**). Liver triglyceride content was also increased by OVX, but
344 DPN treatment did not alter this content significantly (**Figure 3C**). Consistently,
345 macrovesicular steatosis was augmented by OVX, also with no effect of ERβ activation
346 promoted by DPN (**Figure 3D**). These effects were not accompanied by significant effects
347 in isolated liver mitochondrial Complex I and Complex II-linked oxygen consumption
348 rates, nor changes in H_2O_2 production (**Supplementary material Figures S3 and S4**).

349 While total lipid content remained unaffected by the treatment, lipidomic
350 profiling showed that DPN treatment reshaped the lipid composition of OVX animals,
351 resulting in a clearer separation between OVX DPN and OVX vehicle groups in the
352 clustering and PCA analyses, meaning that DPN treatment induced a clear separate
353 clustering of the OVX group (**Figure 3F and G**). DPN promoted a decrease in
354 phospholipids (**Figure 3H-K**) and free cholesterol (FC) (**Figure 3L**) and an increase in
355 cholesteryl esters (CE) (**Figure 3M**). Total acylcarnitines (AC) were also decreased,
356 including AC (10:0), a medium-chain acylcarnitine (**Figure 3N and O**). Analyzing CE
357 species and individual fatty acid (FA) chains in triglycerides uncovered that OVX
358 promoted an increase in saturated and monounsaturated CE and TG fatty acids, with a
359 decrease in polyunsaturated and highly unsaturated FAs (**Figure 3P**). In OVX animals,
360 DPN increased mono, poly and highly unsaturated CE species, while exerting a modest
361 effect on TG species. Overall, these findings indicate that DPN promotes significant
362 lipidome remodeling specific to OVX animals.

363 ### 3.4. Selective ERβ activation remodels hepatocyte lipid profiles *in situ*

364 Overall, results in the animals suggest that OVX promotes large metabolic
365 modifications, resulting in marked unfavorable changes in circulating lipids, liver lipids,
366 and hepatic-derived ketones, in a manner prevented by DPN. This effect was not
367 explained by a direct effect on mitochondria studied in isolation, as assessed in
368 organelles from the tissue of the treated animals (**Supplementary material Figures S3**
369 **and S4**). However, these outcomes could be related to alterations in mitochondrial
370 metabolism *in situ* which depend on cytosolic signaling, and that would not be
371 conserved in experiments with isolated mitochondria. To overcome this limitation, we
372 established a cell model using hepatocytes (AML-12 cells) in which key metabolic
373 features associated with OVX were mimicked by submitting the cells to high glucose
374 combined with palmitate, and the effects of selective ERβ activation were verified by
375 treatment with 0.1 or 1 nM DPN (**Figure 4**).

376 The exposure of hepatocyte cells to high glucose and palmitate (HGP) led to the
377 accumulation of lipid droplets (LD; **Figure 4A**), with higher numbers of LDs (**Figure 4B**)
378 and higher area of LDs per cell (**Figure 4C**), in a manner unaffected by the presence of
379 DPN. This result mirrors effects of DPN on OVX rat livers. Using maximal projection, we
380 quantified LD surface area (exchange surface, **Figure 4D**), and found it significantly
381 increased after DPN treatment, suggesting an effect of DPN on the LD profile.
382 Furthermore, HGP cells presented increased ketone secretion, in a manner prevented
383 by DPN (**Figure 4E** and **4F**), once again mirroring effects seen in OVX animals. Thus, the
384 HGP hepatocyte model presents similar effects to OVX and responds equally to ERβ
385 activation, validating its use in uncovering mechanisms involved in this metabolic
386 modulation, and indicating that the drug acts directly on liver cells.

387 We then conducted extracellular metabolic flux analysis in these hepatocytes
388 using the Seahorse system, quantifying basal (**Figure 5A**), ATP-linked (Oligomycin-
389 inhibited, **Figure 5B**), and maximal (Uncoupler-induced, **Figure 5C**) oxygen consumption
390 rates under typical "Mitochondrial Stress-Test" conditions in which glucose is used as
391 the main added extracellular substrate. All these parameters were decreased in cells
392 submitted to HGP relative to low glucose controls (LGB), with a tendency toward some

393 reversal of these changes by DPN, although results were not consistent in all
394 concentrations and conditions.

395 We then quantified components of the oxidative phosphorylation machinery
396 through western blot analysis using the Total OxPhos antibody mix (a typical blot is
397 shown in **Figure 5D**). With the exception of CI, OXPHOS complexes as well as inner
398 mitochondrial membrane marker protein Tim 23 did not change in HGP, nor with DPN
399 treatment (**Figure 5E-J**). Interestingly, DPN decreased Complex I protein levels (**Figure**
400 **5E**). Pyruvate dehydrogenase (PDH, **Figure 5K** and **5L**) levels remained unchanged, a
401 result that does not explain the increase in oxygen consumption rates promoted by this
402 drug. When looking at other metabolic checkpoints, we found that and DPN did not
403 significantly alter carnitine palmitoyltransferase 2 (CPT2, **Figure 5M**) or electron transfer
404 flavoprotein subunit alpha (ETFA, **Figure 5N**) levels, showing that does not affect
405 quantities of components of fatty acid oxidation. These results indicate that the changes
406 in metabolic fluxes in the presence of DPN involve modulation of metabolic rates rather
407 than control of the amounts of enzymes at the metabolic checkpoints involved.

408 3.5. ERβ selective activation modulates substrate dependence and 409 metabolic flexibility in hepatocytes

410 We saw changes in lipid composition promoted by DPN both *in vitro* and *in vivo*,
411 but no overt changes in mitochondrial oxygen consumption nor composition compatible
412 with changes in metabolism promoted by DPN. Indeed, while the "Stress Test"
413 conducted in Figure 5 can give important information regarding metabolic state, it does
414 not typically include added fatty acids as substrates, nor measure specific substrate
415 oxidation capacity, dependency or flexibility.

416 Extracellular flux measurements can be designed to evaluate the participation of
417 different metabolic pathways in intact cells by following the effects of inhibitors of
418 different metabolic pathways, alone or in combination. We used UK5099, a
419 mitochondrial pyruvate carrier inhibitor, to specifically inhibit complete glucose
420 oxidation (generating pyruvate, which enters mitochondria), Etomoxir (a carnitine
421 palmitoyl transferase inhibitor) to prevent uptake of fatty acids into mitochondria, and
422 BPTES, a glutaminase inhibitor, to assess the roles of carbohydrate, fatty acid, and amino

423 acid oxidation on metabolic fluxes in hepatocytes (**Figure 6A**). With sequential additions
424 of the inhibitors alone or in combination, the dependence and capacity of each pathway
425 can be assessed: dependence is evaluated by inhibiting the target pathway first, then
426 the other pathways, while capacity is evaluated by inhibiting alternate pathways first,
427 followed by the target pathway (**Figure 6A**). Finally, metabolic flexibility can be
428 calculated as the difference between dependence and capacity. Experiments were done
429 in parallel for two concentrations of DPN (0.1 and 1 nM) due to the number of samples
430 needed, in order to conduct controls in parallel for the same sample.

431 Overall (**Figure 6B-S**), we found that nutrient overload with the HGP protocol did
432 not increase the capacity to oxidize pyruvate, glutamine, or palmitate relative to low
433 glucose (LGB) conditions (panels **6C**, **6F**, **6I**, **6L**, **6O**, and **6R**). Conversely, the dependence
434 on the oxidation of glutamine (**Figures 6H** and **6K**) and pyruvate (**Figures 6B** and **6E**)
435 increased under HGP conditions, leading to a reduced metabolic flexibility (**Figures 6D**,
436 **6G**, **6J** and **6M**). Interestingly, by significantly increasing dependence (**Figures 6B**, **6E**, **6N**
437 and **6Q**) on palmitate (**Figures 6P** and **6S**) and pyruvate (**Figures 6D** and **6G**), DPN further
438 reduced flexibility on these substrates.

439 Together, these metabolic flux quantifications demonstrate that selective ERβ
440 activation by DPN in hepatocytes promotes complete mitochondrial oxidation of
441 carbohydrate-derived pyruvate and fat-derived palmitate, a result compatible with the
442 fact that it decreases VLDL, triglycerides, fatty acids, and ketones *in vivo*, and promotes
443 lipid droplet remodeling with enhanced exchange surface *in vitro*.

444

445 ## 4. DISCUSSION

446 Estrogens modulate growth and function of the reproductive tissues, effects
447 which can also be achieved in postmenopause by treatment with classical estrogen
448 receptor agonists. Non-selective estrogen receptor agonists also have metabolic effects,
449 at least partially reversing the undesirable metabolic impacts of menopause (8–10).
450 However, these beneficial results are often unachievable in post-menopausal women
451 who have predisposition toward hormone-responsive cancers, and therefore are not

452 candidates for classic hormone replacement therapy. In this sense, it is of interest to
453 understand the metabolic impact of selective ERβ activation, which is not associated
454 with increased cancer risk (23–28). Fittingly, we found that the *in vivo* treatment with
455 the selective ERβ agonist DPN had no change in wet uterus weights, a result in line with
456 existing literature suggesting that ERβ does not exert trophic effects on the reproductive
457 organ in rodents (44,45), nor influence the hypothalamic-pituitary-gonadal axis (46).

458 A well-documented consequence of estradiol deficiency on energy metabolism
459 is persistent weight gain, not always correlated with food intake (20,47,48). Indeed, we
460 find that OVX animals exhibited marked weight gain beginning the first week post-
461 ovariectomy, which remained pronounced until the experimental endpoint (30 days).
462 Body weight gain per caloric intake was elevated in OVX animals, indicating increased
463 energy conversion efficiency induced by estradiol deficiency. Selective ERβ activation
464 with DPN had no effect on body weight gain or weight gain relative to caloric intake in
465 OVX animals, a finding consistent with a prior study showing that ERβ agonists do not
466 significantly affect body weight (17).

467 Although the ERβ agonist did not influence body weight, marked changes were
468 observed in glucose and lipid metabolism and content after treatment was introduced
469 post-OVX. OVX induced enhanced basal glucose levels, accompanied by changes in
470 pancreatic islet size and circularity. OVX also increased WATr weight and elevated serum
471 cholesterol, LDL, VLDL, triglycerides, and fatty acids - confirming the establishment of an
472 energy overload state induced by estradiol deficiency, characterized in previous
473 literature by elevated fasting glucose, development of insulin resistance (20), increased
474 white adipose tissue mass, and a disrupted circulating lipid profile (48). DPN treatment
475 did not alter glucose tolerance assessed in GTT, but restored basal glucose levels in OVX
476 animals to those observed in controls. DPN also improved islet circularity, preserving
477 physiological pancreatic islet morphology. Moreover, treatment with DPN decreased
478 WATr weight and adipocyte areas in both control and OVX animals, accompanied by
479 improvements in serum cholesterol, VLDL, triglycerides, and FFAs. These data
480 demonstrate that selective ERβ activation, even after estradiol deficiency
481 establishment, can restore critical markers of metabolic disease risk, improving both

482 glucose and lipid homeostasis, in many cases to levels indistinguishable from non-OVX
483 controls.

484 The effects on glucose homeostasis and islet morphology suggest DPN may also
485 exert direct actions on the endocrine pancreas. *In vitro* studies suggest that ERβ, along
486 with ERα and GPER, enhances β-cell survival and function, with ERβ contributing toward
487 apoptosis prevention and K_{ATP} inhibition mimicry (49,50). ERβ$^{-/-}$ mice showed delayed
488 first-phase insulin release following glucose stimulation, but with no changes in basal
489 glucose levels (51). Another study found that DPN did not significantly affect glucose or
490 glycated hemoglobin (HbA1c) in OVX Sprague-Dawley rats (52). Conversely, an ERβ
491 agonist decreased serum glucose levels and improved β-cell function in high fat-fed mice
492 (53), leading to the conclusion that the direct effects of the receptor on β-cells seem to
493 be dependent on the metabolic state and animal model.

494 Visceral adiposity reduction may explain decreased circulating FFAs promoted by
495 DPN treatment observed in our *in vivo* model, as visceral fat exhibits high lipolytic
496 activity, linked to a detrimental cardiovascular profile and β-cell dysfunction (54–56).
497 Indeed, ERβ activation may promote adipose tissue remodeling (17). In male rats, ERβ
498 agonist treatment shifted fat distribution from visceral to subcutaneous without
499 affecting body weight - a pattern associated with reduced lipolytic activity and improved
500 insulin sensitivity (17). In OVX females, ERβ agonists prevented WAT gain, enhanced lean
501 mass (57), reduced LDL, and improved hepatic insulin sensitivity under high-fat diet
502 conditions (53). We found that serum β-hydroxybutyrate levels followed the same
503 pattern as FFAs - increased in OVX animals and fully restored to control levels after DPN
504 treatment. As incomplete lipid oxidation to acetyl CoA is associated with hepatic ketone
505 body production (58,59), these findings implicate the liver, alongside the adipose tissue
506 and endocrine pancreas, in the beneficial metabolic effects observed with ERβ activation
507 *in vivo.* Given the liver's central role in metabolism, and the scarcity of ERβ-focused liver
508 studies, we investigated hepatic metabolic status in OVX females.

509 We found that OVX induced significant changes in liver metabolism, with
510 increased glycogen and lipid accumulation, suggesting substrate overload and enhanced
511 storage signaling. Notably, the GTT curve did not differ between OVX and control
512 animals, suggesting a similar insulin sensitivity. However, increased ketone production

513 alongside lipid accumulation suggests early-stage metabolic-associated fatty liver
514 disease (MASLD)-like decompensation (60,61), although macrovesicular steatosis in our
515 samples remained within physiological levels (39). In line with this, the increase in
516 monosaturated and the decrease in highly unsaturated cholesteryl ester accompanied
517 by the same pattern in triglyceride fatty acid species in OVX (62) indicates an ongoing
518 dysregulation of hepatic lipid processing. Interestingly, DPN treatment promoted a
519 lipidome shift toward a protective profile, characterized by decreased FFAs and
520 increased esterified cholesterol ester species, particularly those containing
521 monounsaturated, polyunsaturated, and highly unsaturated fatty acids. This aligns with
522 literature showing ERβ agonists reduce saturated fatty acids while increasing
523 unsaturated species in high-fat diet models of non-ovariectomized females and in obese
524 male mice (17,53), and shows the potential of ERβ as a target in metabolic overload
525 under estradiol-deficient conditions.

526 We also assessed mitochondrial function in freshly isolated liver mitochondria.
527 Both state 3 (phosphorylating) and state 4 (proton-leak dependent) oxygen
528 consumption were elevated in St3 consumption (CI and CII-linked) in OVX animals,
529 indicating higher electron transport rates and, but reduced coupling efficiency (CII-
530 linked) between oxygen consumption and ATP synthesis (**Figure S3**). This inefficiency is
531 a known feature of estradiol deficiency and is recoverable via non-selective estradiol
532 treatment (63,64), implicating estrogen receptors in mitochondrial regulation (64–66).
533 Fittingly, our results showed that DPN-treated OVX animals did not have differences in
534 mitochondrial oxygen coupling rate when compared to controls, indicating that the
535 treatment restores these oxidative phosphorylation parameters. These results are
536 different from previously reported estradiol (non-selective) effects (64–66) and suggest
537 ERβ may have distinct impacts on mitochondrial respiration.

538 While ERβ mitochondrial effects in liver had not been uncovered previously,
539 some work has shown that ERβ appears to be involved in hepatic lipid metabolism, and
540 may attenuate MASLD progression (57,67), despite its lower expression levels (22,57) in
541 this organ. Our findings indicate that OVX induced lipid accumulation and mild steatosis
542 without structural liver damage, indicating subclinical metabolic imbalance. DPN
543 treatment did not alter total liver lipid quantities nor histological macrovesicular

544 steatosis, but profoundly shifted lipid species composition. ERβ activation thus triggers
545 a lipidomic shift that favors a protective profile, with the conversion of toxic free fatty
546 acids into triglycerides, acting as a buffering mechanism that correlates with improved
547 serological outcomes (68,69).

548 To understand the changes in metabolism happening in liver cells in terms of
549 specific metabolic modulation, we also conducted *in vitro* studies with hepatocytes. Our
550 model reproduced the effects of nutrient overload seen *in vivo*, with accumulation of
551 lipid droplets and enhanced ketone release. As seen *in vivo*, DPN prevented ketone
552 production (70,71), but not lipid accumulation. A notable finding *in vivo* was the
553 decrease in several phospholipid species, which can be associated with the presence of
554 supersized lipid droplets (LDs), that have lower exchange surfaces and may be less
555 accessible for metabolization, thereby impairing lipid oxidation (72,73). Interestingly,
556 quantification *in vitro* revealed that the DPN treatment increased exchange surface area
557 of the LDs, suggesting enhanced accessibility for metabolization. Overall, our data show
558 that ERβ activation directly regulates the specific types of FFAs available for oxidation
559 within hepatocytes. By modulating this lipid supply, the treatment prevents acetyl-CoA
560 overload, the primary substrate for ketogenesis. As effects can be reproduced in liver
561 cells, these metabolic shifts are driven by direct cellular mechanisms rather than by
562 systemic effects of the drug.

563 Interestingly, estradiol is known to enhance hepatic oxidative machinery and
564 substrate oxidation (74,75), a result that is partially compatible with our results
565 suggesting ERβ may promote increased dependence and decreased flexibility of full
566 oxidation of carbohydrate-derived pyruvate and the fatty acid palmitate. This switch
567 promotes complete acetyl-CoA oxidation, accompanied by decreased long-chain
568 acylcarnitines, explaining reduced incomplete lipid oxidation and ketone body release
569 under nutrient overload seen in both our *in vitro* and *in vivo* models (74).

570 Overall, we find that ERβ activation promotes specific metabolic reconfiguration
571 in liver cells that impact on *in vivo* lipid and glucose metabolism, promoting improved
572 systemic glucose and lipid homeostasis as well as positively modulating the liver
573 lipidome, despite persistent energy overload seen in the absence of estrogens. These
574 findings highlight ERβ activation as a promising alternative to non-selective estradiol

therapy, particularly for postmenopausal women with established metabolic imbalances.

ACKNOWLEDGEMENTS

The authors acknowledge Professor Vilma Regina Martins for intellectual contributions. We also thank Silvânia M. P. Neves and animal facility crew for excellent animal care, Sirley Mendes de Oliveira for technical support and Mario Costa Cruz (CONFOCAL – CEFAP facility) for histological image capturing.

FUNDING SOURCES

Supported by the *Fundação de Amparo à Pesquisa do Estado de São Paulo* (FAPESP) under grant numbers 13/07937-8, 2020/06970-5, 2021/04781-3, and 24/13461-0, *Conselho Nacional de Desenvolvimento Científico e Tecnológico* (CNPq) 408213/2024-8 and 303886/2021-8, as well as *Coordenação de Aperfeiçoamento de Pessoal de Nível Superior* (CAPES) line 001.

DISCLOSURES

The authors declare no conflicts of interest.

DATA AVAILABILITY

Full data has been deposited in Zenodo: 10.5281/zenodo.19487483

AUTHOR CONTRIBUTIONS

DSR conceived this research, analyzed data, performed experiments, interpreted results, prepared figures, and drafted the manuscript, under supervision of AJK; EAVB,

600 ELV, MICQ, CCCS, MY, and SM performed *in vivo* experiments and interpreted results;
601 MPTC performed *in vitro* experiments and interpreted results. All authors revised and
602 approved the final version of the manuscript.

603 **FIGURE CAPTIONS**

604 **Figure 1. ERβ agonist modulates glucose homeostasis in ovariectomized (OVX) female**
605 **Wistar rats.** Experimental protocol (**A**). Uterus weight (**B**), body weight gain (**C**), final
606 body weight gain per caloric intake (**D**). Week 1 (**E**), week 3 (**F**), week 5 (**G**) GTT AUC.
607 Week 1 (**H**), week 3 (**I**), week 5 (**J**) basal glucose levels. Representative islet histology (**K**),
608 pancreatic islet size distribution (**L**), pancreas circularity (**M**). Groups were compared by
609 two-way ANOVA followed by Tukey posttest. N = 5-6 (A-J) n = 5 (K-M). Significances were
610 considered at $p < 0.05$.

611 **Figure 2. ERβ agonist modulates lipid homeostasis in ovariectomized (OVX) female**
612 **Wistar rats.** Representative WATr histology (**A**). Retroperitoneal white adipose tissue
613 (WATr) weight (**B**), WATr adipocyte area (**C**), serum cholesterol (**D**), HDL (**E**), LDL (**F**), VLDL
614 (**G**), triglycerides (**H**), non-esterified fatty acids (**I**), β-hydroxybutyrate (**J**). Groups were
615 compared by two-way ANOVA followed by Tukey posttest. N = 5. Significances were
616 considered at $p < 0.05$.

617 **Figure 3. Post-OVX liver metabolism is modulated by selective ERβ activation.**
618 Representative liver histology (**A**), liver glycogen (**B**), triglycerides (**C**), macrovesicular
619 steatosis (**D**), liver weight (**E**). Lipidomic Principal Component Analysis (**F**) clustering (**G**),
620 and quantification of phospholipids (**H-K**), free cholesterol (**L**), cholesteryl esters (**M**),
621 acylcarnitine (**N** and **O**), CE and TG associated lipids (**P**) were assessed. Groups were
622 compared by two-way ANOVA followed by Tukey posttest. N = 5 (A-D) n = 6-7 (E-J).
623 Significances were considered at $p < 0.05$

624 **Figure 4. Selective ERβ activation remodels hepatocyte lipid profiles *in situ*.**
625 Representative images of mitochondrial network and lipid droplets using Mitotracker
626 deep red (gray) and BODIPY (yellow) (**A**); lipid droplets count (**B**) and area (**C**) per cell
627 and Exchange surface (**D**). β- hydroxybutyrate release to the culture medium after 24 h
628 of treatment (**D** and **E**). Groups were compared by one-way ANOVA. n = 4-5.
629 Significances were considered at $p < 0.05$.

630 **Figure 5. ERβ agonist effects on oxygen consumption, levels of mitochondrial oxidative**
631 **phosphorylation components and metabolic checkpoints**. Basal (**A**), ATP-linked (**B**), and
632 maximal (**C**) oxygen consumption rates. Representative blot of oxidative
633 phosphorylation components using total Oxphos antibody mix (**D**) and TIM23 as internal
634 control. Quantification of protein levels of mitochondrial complexes I, II, III, IV, and V (**E-**
635 **I**). Representative blots (**K**) and quantifications of pyruvate dehydrogenase (PDH, **L**),
636 Carnitine palmitoyltransferase II (CPT2, **M**), electron transfer flavoprotein subunit alpha
637 (EFTA, **N**). Ponceau staining was used for normalization in L-M. Groups were compared
638 by one-way ANOVA. n = 3-5. Significances were considered at $p < 0.05$.

639 **Figure 6. ERβ activation modulates substrate oxidation dependence and flexibility**
640 **under conditions of energy overload**. Oxygen consumption rates (OCR) were measured
641 under basal conditions, and after the injection of 7 µM Etomoxir (CPT1 inhibitor), 6 µM
642 UK5099 (mitochondrial pyruvate carrier inhibitor) and/or 8 µM BPTES (glutaminase
643 inhibitor), as indicated, to measure dependence and capacity (**Panel A**, adapted from
644 Agilent (76), created with Biorender). Capacity was measured after injecting all
645 inhibitors except for the target oxidative pathway inhibitor. Dependence was expressed
646 as the target substrate per all inhibitor response ratio. Capacity was expressed as the
647 alternative substrates' response per all inhibitors' response ratio. Flexibility is the
648 difference between capacity and dependence. Values were quantified for the different
649 substrates (Pyruvate, **B-G**; Glutamine, **H-M**; and Palmitate, **N-S**) and using two DPN
650 concentrations, as shown. Groups were compared by one-way ANOVA. n = 3-4.
651 Significances were considered at $p < 0.05$.

REFERENCES

(1) Mahboobifard F, Pourgholami MH, Jorjani M, Dargahi L, Amiri M, Sadeghi S, et al. Estrogen as a key regulator of energy homeostasis and metabolic health. Biomed Pharmacother. 2022 Dec;156:113808.

(2) Barros RPA, Gustafsson JÅ. Estrogen receptors and the metabolic network. Cell Metab. 2011;14(3):289–99.

(3) Cheng Y, Zhu H, Ren J, Wu HY, Yu JE, Jin LY, et al. Follicle-stimulating hormone orchestrates glucose-stimulated insulin secretion of pancreatic islets. Nat Commun. 2023 Nov;14(1):6991.

(4) Poehlman ET, Toth MJ, Gardner AW. Changes in energy balance and body composition at menopause: A controlled longitudinal study. Ann Intern Med. 1995;123(9):673–5.

(5) Lobo RA. Metabolic syndrome after menopause and the role of hormones. Maturitas. 2008;60(1):10–8.

(6) Poitout V, Robertson RP. Glucolipotoxicity: Fuel excess and β-cell dysfunction. Endocr Rev. 2008;29(3):351–66.

(7) Cerqueira FM, Chausse B, Baranovski BM, Liesa M, Lewis EC, Shirihai OS, et al. Diluted serum from calorie-restricted animals promotes mitochondrial β-cell adaptations and protect against glucolipotoxicity. FEBS J. 2016 Mar;283(5):822–33.

(8) Cox-York KA, Erickson CB, Pereira RI, Bessesen DH, Van Pelt RE. Region-specific effects of oestradiol on adipose-derived stem cell differentiation in post-menopausal women. J Cell Mol Med. 2017;21(4):677–84.

(9) Livingstone C, Collison M. Sex steroids and insulin resistance. Clin Sci. 2002;102(2):151–66.

(10) De Los Angeles Carrasco-Ruiz M, Hernandez-Aragon LG, Chavez-Rios JR, Rodriguez-Antolin J, Pacheco P, Martinez-Gomez M, et al. High estradiol differentially affects the expression of the glucose transporter type 4 in pelvic floor muscles of rats. Int Neurourol J. 2018;22(3):161–8.

(11) Leitman DC, Paruthiyil S, Yuan C, Herber CB, Olshansky M, Tagliaferri M, et al. Tissue-specific regulation of genes by estrogen receptors. Semin Reprod Med. 2012;30(1):14–22.

(12) Cedó L, Reddy ST, Mato E, Blanco-Vaca F, Escolà-Gil JC. HDL and LDL: Potential New Players in Breast Cancer Development. J Clin Med. 2019;8(6):853.

(13) Tesarik J, Mendoza C. Nongenomic effects of 17 beta-estradiol on maturing human oocytes: relationship to oocyte developmental potential. J Clin Endocrinol Metab. 1995 Apr;80(4):1438–43.

(14) Kelly MJ, Wagner EJ. Estrogen Modulation of G-protein-coupled Receptors. Trends Endocrinol Metab. 1999;10(9):369–74.

(15) Musatov S, Chen W, Pfaff DW, Mobbs CV, Yang XJ, Clegg DJ, et al. Silencing of estrogen receptor alpha in the ventromedial nucleus of hypothalamus leads to metabolic syndrome. Proc Natl Acad Sci U S A. 2007 Feb;104(7):2501–6.

(16) Barreto-Andrade JN, de Fátima LA, Campello RS, Guedes JAC, de Freitas HS, Okamoto MM, et al. Estrogen receptor 1 (ESR1) enhances Slc2a4/GLUT4 expression by a SP1 cooperative mechanism. Int J Med Sci. 2018;15(12):1320–8.

(17) González-Granillo M, Savva C, Li X, Ghosh Laskar M, Angelin B, Gustafsson JÅ, et al. Selective estrogen receptor (ER)β activation provokes a redistribution of fat mass and modifies hepatic triglyceride composition in obese male mice. Mol Cell Endocrinol. 2020;502:110672.

(18) Barros RPA, Machado UF, Warner M, Gustafsson JA. Muscle GLUT4 regulation by estrogen receptors ERbeta and ERalpha. Proc Natl Acad Sci U S A. 2006 Jan;103(5):1605–8.

(19) Buniam J, Chukijrungroat N, Khamphaya T, Weerachayaphorn J, Saengsirisuwan V. Estrogen and voluntary exercise attenuate cardiometabolic syndrome and hepatic steatosis in ovariectomized rats fed a high-fat high-fructose diet. Am J Physiol Endocrinol Metab. 2019;316(5):E908–21.

(20) Bailey CJ, Ahmed-Sorour H. Role of ovarian hormones in the long-term control of glucose homeostasis - Effects on insulin secretion. Diabetologia. 1980;19(5):475–81.

(21) Gao H, Fält S, Sandelin A, Gustafsson JÅ, Dahlman-Wright K. Genome-wide identification of estrogen receptor α-binding sites in mouse liver. Mol Endocrinol. 2008;22(1):10–22.

(22) Foryst-Ludwig A, Clemenz M, Hohmann S, Hartge M, Sprang C, Frost N, et al. Metabolic Actions of Estrogen Receptor Beta (ERβ) are Mediated by a Negative Cross-Talk with PPARγ. PLOS Genet. 2008 Jun 27;4(6):e1000108.

(23) Arnal JF, Lenfant F, Flouriot G, Tremollières F, Laurell H, Fontaine C, et al. From in vivo gene targeting of oestrogen receptors to optimization of their modulation in menopause. Br J Pharmacol. 2012;165(1):57–66.

(24) Radde BN, Ivanova MM, Mai HX, Salabei JK, Hill BG, Klinge CM. Bioenergetic differences between MCF-7 and T47D breast cancer cells and their regulation by oestradiol and tamoxifen. Biochem J. 2015 Jan;465(1):49–61.

(25) Radde BN, Ivanova MM, Mai HX, Alizadeh-Rad N, Piell K, Van Hoose P, et al. Nuclear respiratory factor-1 and bioenergetics in tamoxifen-resistant breast cancer cells. Exp Cell Res. 2016 Sep;347(1):222–31.

(26) Salama SA, Mohammad MA, Diaz-Arrastia CR, Kamel MW, Kilic GS, Ndofor BT, et al. Estradiol-17β upregulates pyruvate kinase M2 expression to coactivate estrogen receptor-α and to integrate metabolic reprogramming with the mitogenic response in endometrial cells. J Clin Endocrinol Metab. 2014 Oct;99(10):3790–9.

(27) Liao TL, Tzeng CR, Yu CL, Wang YP, Kao SH. Estrogen receptor-β in mitochondria: implications for mitochondrial bioenergetics and tumorigenesis. Ann N Y Acad Sci. 2015;1350(1):52-60.

(28) Caruntu C, Mirica A, Roșca AE, Mirica R, Caruntu A, Tampa M, et al. The role of estrogens and estrogen receptors in melanoma development and progression. Acta Endocrinol (Copenh). 2016;12(2):234–41.

(29) Leary S, Underwood W, Anthony R, Cartner S. AVMA Guidelines for the Euthanasia of Animals: 2013 Edition. American Veterinary Medical Association; 2013. 98 p.

(30) National Research Council. Guide for the Care and Use of Laboratory Animals: Eighth Edition. Washington, DC: The National Academies Press; 2011.

(31) du Sert NP, Hurst V, Ahluwalia A, Alam S, Avey MT, Baker M, et al. The ARRIVE guidelines 2.0: Updated guidelines for reporting animal research. PLoS Biol. 2020 Jul 1;18(7):e3000410.

(32) Idris AI. Ovariectomy/orchidectomy in rodents. Methods Mol Biol. 2012;816:545–51.

(33) Langford DJ, Bailey AL, Chanda ML, Clarke SE, Drummond TE, Echols S, et al. Coding of facial expressions of pain in the laboratory mouse. Nat Methods. 2010;7(6):447–9.

(34) Munhoz AC, Serna JDC, Vilas-Boas EA, Caldeira da Silva CC, Santos TG, Mosele FC, et al. Adiponectin reverses β-Cell damage and impaired insulin secretion induced by obesity. Aging Cell. 2023 Jun;22(6):e13827.

(35) Huang S, Li Z, Sun Y, Chen B, Jiang Y, Hong F. Increased CD34 in pancreatic islet negatively predict islet β-cell decrease in type1 diabetes model. Front Physiol. 2022;13:1032774.

(36) Villaça CBP, de Paula CC, de Oliveira CC, Vilas-Boas EA, Dos Santos-Silva JC, de Oliveira SF, et al. Beneficial effects of physical exercise for β-cell maintenance in a type 1 diabetes mellitus animal model. Exp Physiol. 2021 Jul;106(7):1482–97.

(37) Palomäki VA, Koivukangas V, Meriläinen S, Lehenkari P, Karttunen TJ. A Straightforward Method for Adipocyte Size and Count Analysis Using Open-source Software QuPath. Adipocyte. 2022;11(1):99–107.

(38) Brunt EM. Nonalcoholic steatohepatitis (NASH): Further expansion of this clinical entity? Liver. 1999;19:263–4.

(39) Brown GT, Kleiner DE. Histopathology of nonalcoholic fatty liver disease and nonalcoholic steatohepatitis. Metabolism. 2016;65(8):1080–6.

(40) Yoshinaga MY, Quintanilha BJ, Chaves-Filho AB, Miyamoto S, Sampaio GR, Rogero MM. Postprandial plasma lipidome responses to a high-fat meal among healthy women. J Nutr Biochem. 2021 Nov;97:108809.

(41) Chong J, Soufan O, Li C, Caraus I, Li S, Bourque G, et al. MetaboAnalyst 4.0: towards more transparent and integrative metabolomics analysis. Nucleic Acids Res. 2018 Jul;46(W1):W486–94.

(42) Vilas-Boas EA, Cabral-Costa JV, Ramos VM, Caldeira da Silva CC, Kowaltowski AJ. Goldilocks calcium concentrations and the regulation of oxidative phosphorylation: Too much, too little, or just right. J Biol Chem. 2023 Mar;299(3):102904.

(43) Kakimoto PA, Serna JDC, de Miranda Ramos V, Zorzano A, Kowaltowski AJ. Increased glycolysis is an early consequence of palmitate lipotoxicity mediated by redox signaling. Redox Biol. 2021 Sep;45:102026.

(44) Malamas MS, Manas ES, McDevitt RE, Gunawan I, Xu ZB, Collini MD, et al. Design and Synthesis of Aryl Diphenolic Azoles as Potent and Selective Estrogen Receptor-β Ligands. J Med Chem. 2004 Oct 1;47(21):5021–40.

(45) Mewshaw RE, Edsall RJ, Yang C, Manas ES, Xu ZB, Henderson RA, et al. ERβ Ligands. 3. Exploiting Two Binding Orientations of the 2-Phenylnaphthalene Scaffold To Achieve ERβ Selectivity. J Med Chem. 2005 Jun 1;48(12):3953–79.

(46) Hewitt SC, Harrell JC, Korach KS. Lessons in estrogen biology from knockout and transgenic animals. Annu Rev Physiol. 2005;67:285–308.

(47) D'Eon TM, Souza SC, Aronovitz M, Obin MS, Fried SK, Greenberg AS. Estrogen Regulation of Adiposity and Fuel Partitioning: Evidence of Genomic and Non-genomic Regulation of Lipogenic and Oxidative Pathways. J Biol Chem. 2005;280(43):35983–91.

(48) Brown LM, Gent L, Davis K, Clegg DJ. Metabolic impact of sex hormones on obesity. Brain Res. 2010;1350:77–85.

(49) Babiloni-Chust I, dos Santos RS, Medina-Gali RM, Perez-Serna AA, Encinar JA, Martinez-Pinna J, et al. G protein-coupled estrogen receptor activation by bisphenol-A disrupts the protection from apoptosis conferred by the estrogen receptors ERα and ERβ in pancreatic beta cells. Environ Int. 2022;164:107250.

(50) Soriano S, Ropero AB, Alonso-Magdalena P, Ripoll C, Quesada I, Gassner B, et al. Rapid Regulation of KATP Channel Activity by 17β-Estradiol in Pancreatic β-Cells Involves the Estrogen Receptor β and the Atrial Natriuretic Peptide Receptor. Mol Endocrinol. 2009 Dec 1;23(12):1973–82.

(51) Barros RPA, Gabbi C, Morani A, Warner M, Gustafsson JÅ. Participation of ERα and ERβ in glucose homeostasis in skeletal muscle and white adipose tissue. Am J Physiol Endocrinol Metab. 2009;297(1):E124–33.

(52) Bansal S, Chopra K. Distinct role of estrogen receptor-alpha and beta on postmenopausal diabetes-induced vascular dysfunction. Gen Comp Endocrinol. 2014;206:51–9.

(53) González-Granillo M, Savva C, Li X, Fitch M, Pedrelli M, Hellerstein M, et al. ERβ activation in obesity improves whole body metabolism via adipose tissue function and enhanced mitochondria biogenesis. Mol Cell Endocrinol. 2019;479:147–58.

(54) Lafontan M, Langin D. Lipolysis and lipid mobilization in human adipose tissue. Prog Lipid Res. 2009;48(5):275–97.

(55) Nielsen S, Guo Z, Johnson CM, Hensrud DD, Jensen MD. Splanchnic lipolysis in human obesity. J Clin Invest. 2004 Jun 1;113(11):1582–8.

(56) Karastergiou K, Smith SR, Greenberg AS, Fried SK. Sex differences in human adipose tissues - The biology of pear shape. Biol Sex Differ. 2012;3(1):13.

(57) Yepuru M, Eswaraka J, Kearbey JD, Barrett CM, Raghow S, Veverka KA, et al. Estrogen receptor-β-selective ligands alleviate high-fat diet- and ovariectomy-induced obesity in mice. J Biol Chem. 2010 Oct 8;285(41):31292–303.

(58) Rosenbloom J. The acetone bodies in diabetes mellitus: influence of low and high protein intake on the excretion of acetone, diacetic acid and beta-oxybutyric acid. JAMA. 1915;65(20):1715–7.

(59) Nelson AB, Queathem ED, Puchalska P, Crawford PA. Metabolic Messengers: ketone bodies. Nat Metab. 2023;5(12):2062–74.

(60) Sunny NE, Parks EJ, Browning JD, Burgess SC. Excessive hepatic mitochondrial TCA cycle and gluconeogenesis in humans with nonalcoholic fatty liver disease. Cell Metab. 2011 Dec 7;14(6):804–10.

(61) Lambert JE, Ramos-Roman MA, Browning JD, Parks EJ. Increased de novo lipogenesis is a distinct characteristic of individuals with nonalcoholic fatty liver disease. Gastroenterology. 2014;146(3):726–35.

(62) Huang DQ, Wong VWS, Rinella ME, Boursier J, Lazarus JV, Yki-Järvinen H, et al. Metabolic dysfunction-associated steatotic liver disease in adults. Nat Rev Dis Primers. 2025;11(1):14.

(63) Fuller KNZ, McCoin CS, Von Schulze AT, Houchen CJ, Choi MA, Thyfault JP. Estradiol treatment or modest exercise improves hepatic health and mitochondrial outcomes in female mice following ovariectomy. Am J Physiol Endocrinol Metab. 2021 Jun;320(6):E1020–31.

(64) Mattingly KA, Ivanova MM, Riggs KA, Wickramasinghe NS, Barch MJ, Klinge CM. Estradiol stimulates transcription of nuclear respiratory factor-1 and increases mitochondrial biogenesis. Mol Endocrinol. 2008 Mar;22(3):609–22.

(65) Nilsen J, Chen S, Irwin RW, Iwamoto SJ, Brinton RD. Estrogen protects neuronal cells from amyloid beta-induced apoptosis via regulation of mitochondrial proteins and function. BMC Neurosci. 2006 Nov 3;7:74.

(66) Gigli I, Bussmann LE. Exercise and ovarian steroid hormones: Their effects on mitochondrial respiration. Life Sci. 2001;68(13):1505-14.

(67) Shin ES, Lee H, Cho SY, Park HW, Lee SJ, Lee TR. Genistein downregulates SREBP-1 regulated gene expression by inhibiting site-1 protease expression in HepG2 cells. J Nutr. 2007;137(7):1727-31.

(68) Listenberger LL, Han X, Lewis SE, Cases S, Farese RV, Ory DS, et al. Triglyceride accumulation protects against fatty acid-induced lipotoxicity. Proc Natl Acad Sci U S A. 2003;100(6):3077-82.

(69) Ricchi M, Odoardi MR, Carulli L, Anzivino C, Ballestri S, Pinetti A, et al. Differential effect of oleic and palmitic acid on lipid accumulation and apoptosis in cultured hepatocytes. J Gastroenterol Hepatol. 2009;24(5):830–40.

(70) Martins-Maciel ER, Campos LB, Salgueiro-Pagadigorria CL, Bracht A, Ishii-Iwamoto EL. Raloxifene affects fatty acid oxidation in livers from ovariectomized rats by acting as a pro-oxidant agent. Toxicol Lett. 2013;217(1):82–9.

(71) Weinstein I, Soler-Argilaga C, Werner HV, Heimberg M. Effects of ethynyloestradiol on the metabolism of [1-14C]oleate by perfused livers and hepatocytes from female rats. Biochem J. 1979;180(2):265-71.

(72) Wölk M, Fedorova M. The lipid droplet lipidome. FEBS Lett. 2024 May 1;598(10):1215–25.

(73) Fei W, Shui G, Zhang Y, Krahmer N, Ferguson C, Kapterian TS, et al. A Role for Phosphatidic Acid in the Formation of “Supersized” Lipid Droplets. PLOS Genet. 2011 Jul 28;7(7):e1002201.

(74) McCoin CS, Knotts TA, Adams SH. Acylcarnitines—old actors auditioning for new roles in metabolic physiology. Nat Rev Endocrinol. 2015;11(10):617–25.

(75) Rettberg JR, Yao J, Brinton RD. Estrogen: A master regulator of bioenergetic systems in the brain and body. Front Neuroendocrinol. 2014;35(1):8–30.

(76) Agilent Technologies. Agilent XF Substrate Oxidation Stress Test Kits User Manual. 2020.

TABLES

Table 1. Antibodies and dilutions

Target	Company	Code	Dilution
Mitochondrial complexes I-V	Abcam	110413	1:1000
Tim23	Cell Signaling	514463	1:500
Pyruvate dehydrogenase (PDH)	Cell Signaling	C54G1	1:1000
Carnitine palmitoyltransferase II (CPT2)	Abcam	18114	1:1000
Electron transfer flavoprotein subunit alpha (ETFA)	Sigma-Aldrich	HPA018990	1:1000

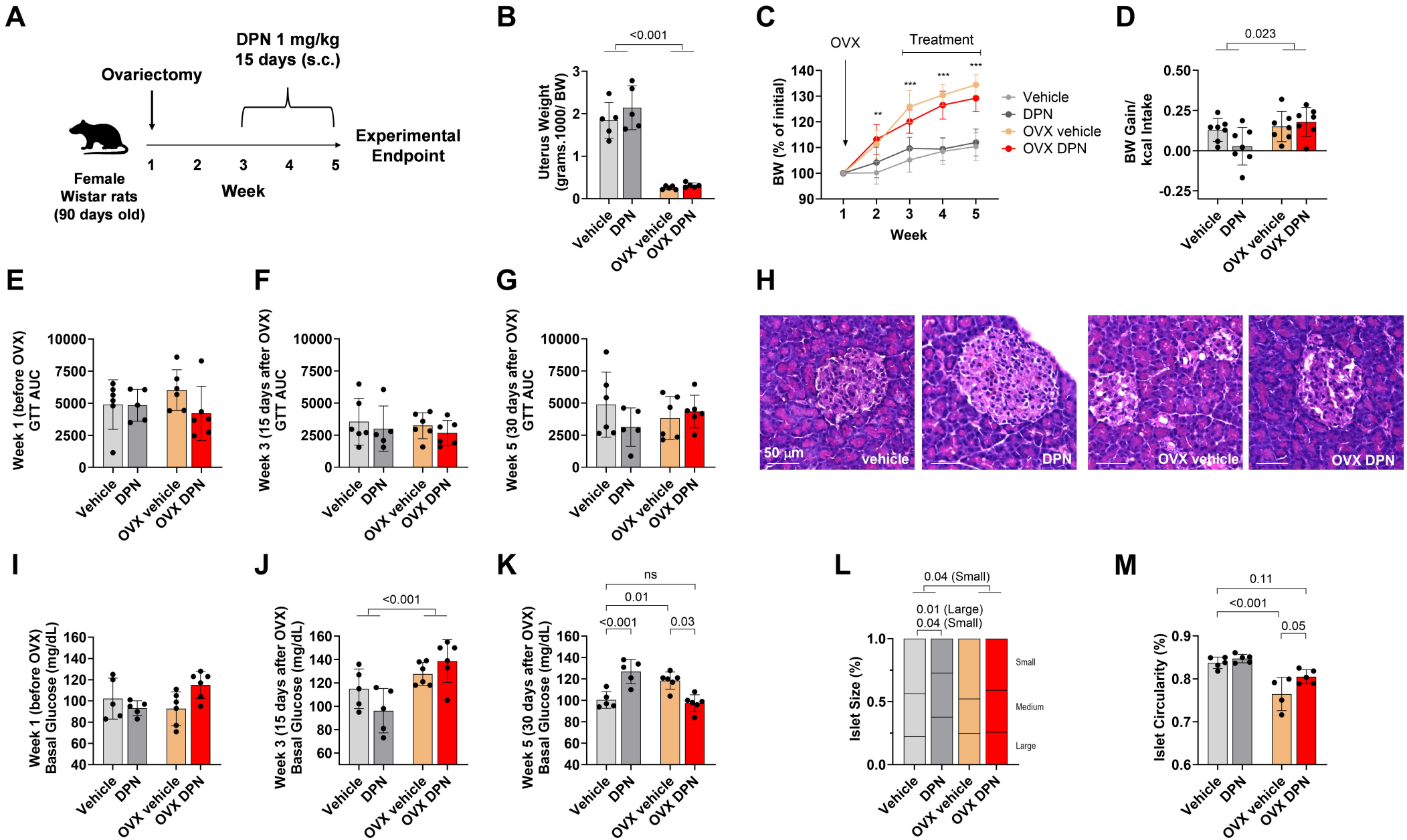
A
DPN 1 mg/kg
15 days (s.c.)
Ovariectomy
Female
Wistar rats
(90 days old)
1
2
3
4
5
Week
Experimental
Endpoint
B
<0.001
Uterus Weight
(grams.1000/ BW)
Vehicle
DPN
OVX vehicle
OVX DPN
C
OVX
Treatment
BW (% of initial)
Week
Vehicle
DPN
OVX vehicle
OVX DPN
D
0.023
BW Gain/
kcal Intake
E
Week 1 (before OVX)
GTT AUC
F
Week 3 (15 days after OVX)
GTT AUC
G
Week 5 (30 days after OVX)
GTT AUC
H
50 µm
vehicle
DPN
OVX vehicle
OVX DPN
I
Week 1 (before OVX)
Basal Glucose (mg/dL)
J
<0.001
Week 3 (15 days after OVX)
Basal Glucose (mg/dL)
K
ns
0.01
<0.001
0.03
Week 5 (30 days after OVX)
Basal Glucose (mg/dL)
L
0.04 (Small)
0.01 (Large)
0.04 (Small)
Islet Size (%)
Small
Medium
Large
M
0.11
<0.001
0.05
Islet Circularity (%)

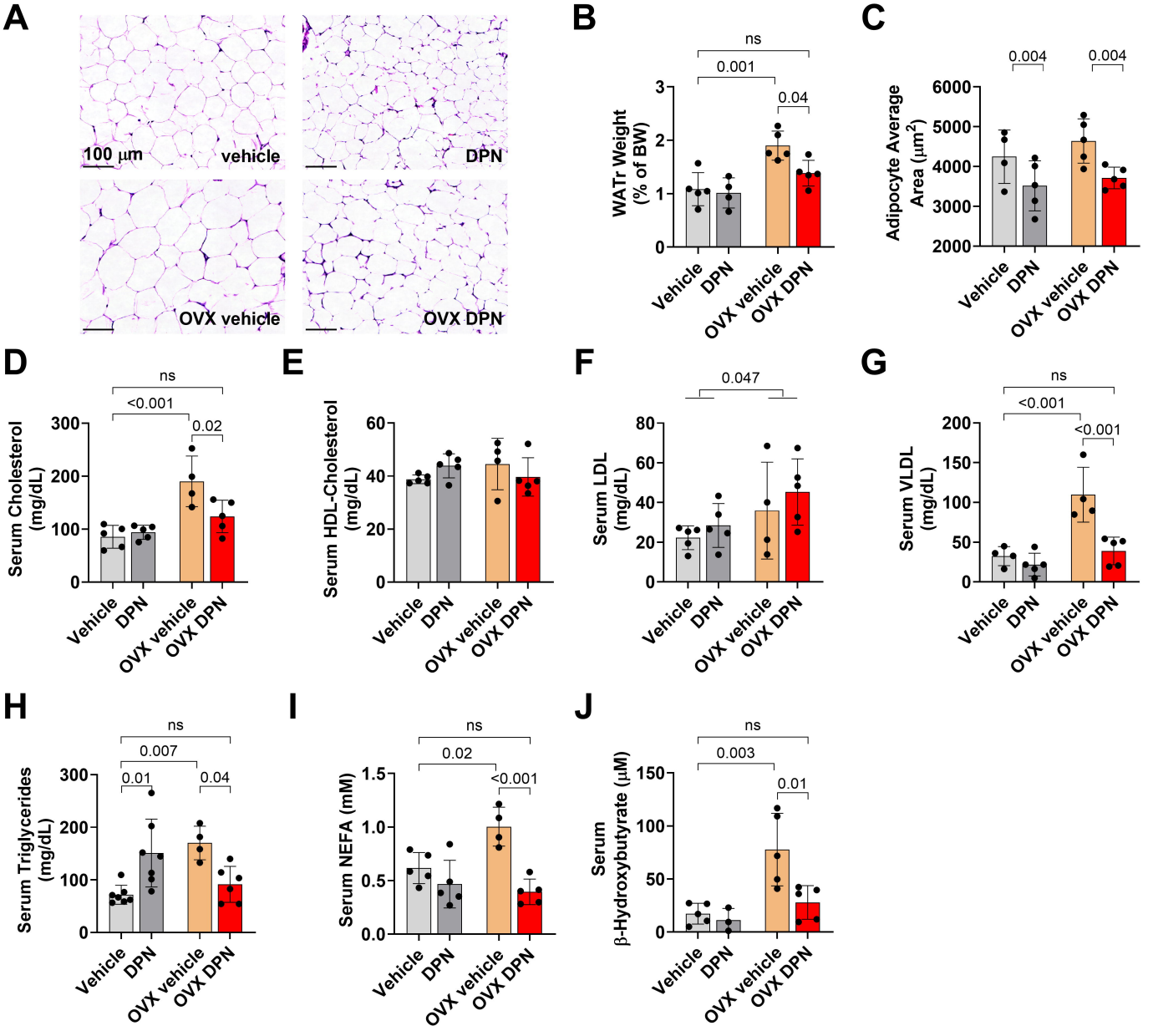
A
100 µm
vehicle
DPN
OVX vehicle
OVX DPN
B
WATr Weight (% of BW)
ns
0.001
0.04
C
Adipocyte Average Area (µm²)
0.004
0.004
D
Serum Cholesterol (mg/dL)
ns
<0.001
0.02
E
Serum HDL-Cholesterol (mg/dL)
F
Serum LDL (mg/dL)
0.047
G
Serum VLDL (mg/dL)
ns
<0.001
<0.001
H
Serum Triglycerides (mg/dL)
ns
0.007
0.01
0.04
I
Serum NEFA (mM)
ns
0.02
<0.001
J
Serum β-Hydroxybutyrate (µM)
ns
0.003
0.01
Vehicle
DPN
OVX vehicle
OVX DPN

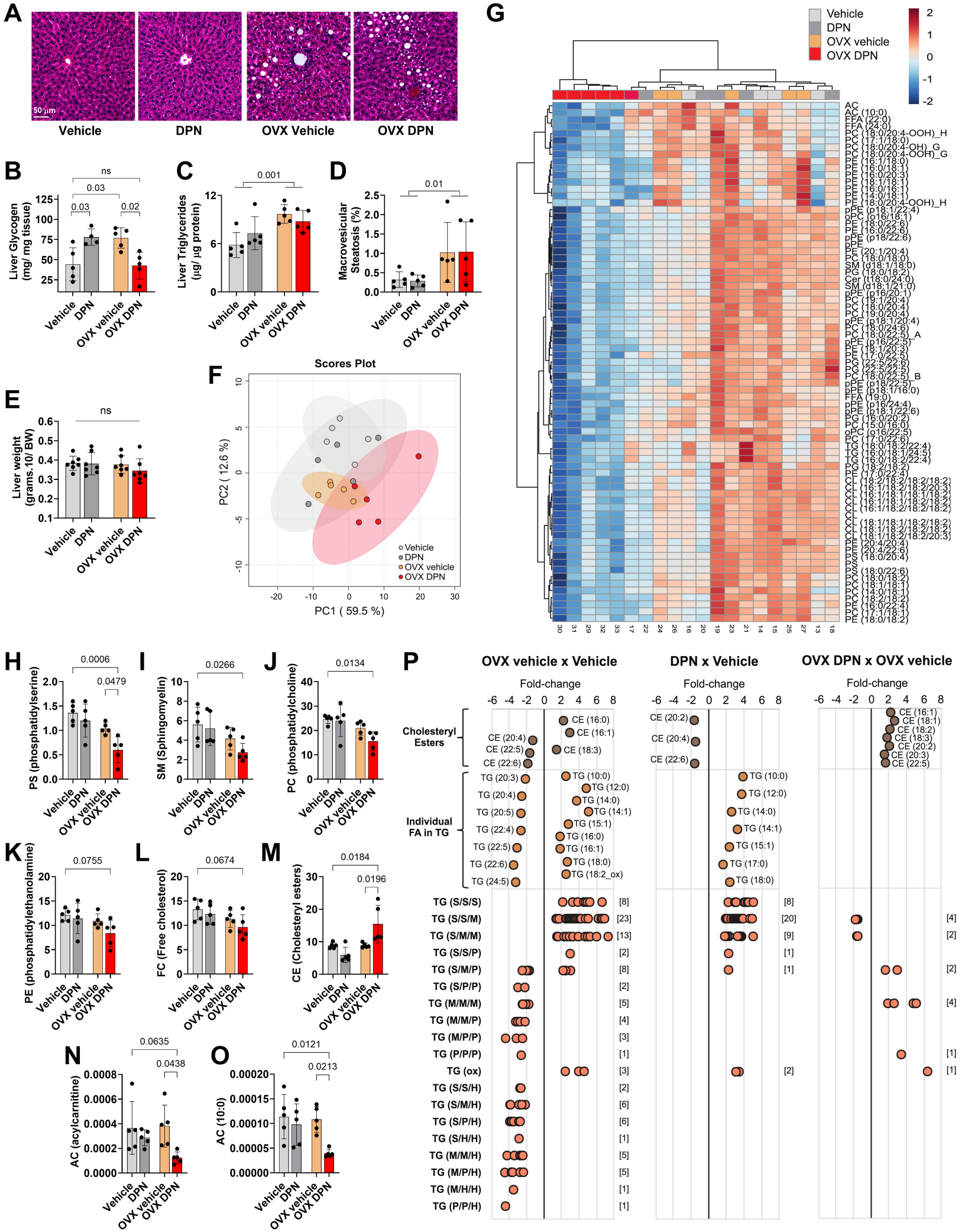
A
50 µm
Vehicle
DPN
OVX Vehicle
OVX DPN
B
Liver Glycogen (mg/ mg tissue)
ns
0.03
0.03
0.02
C
Liver Triglycerides (µg/ µg protein)
0.001
D
Macrovesicular Steatosis (%)
0.01
E
Liver weight (grams.10/ BW)
ns
F
Scores Plot
PC1 (59.5 %)
PC2 (12.6 %)
Vehicle
DPN
OVX vehicle
OVX DPN
G
Vehicle
DPN
OVX vehicle
OVX DPN
H
PS (phosphatidylserine)
0.0006
0.0479
I
SM (Sphingomyelin)
0.0266
J
PC (phosphatidylcholine)
0.0134
K
PE (phosphatidylethanolamine)
0.0755
L
FC (Free cholesterol)
0.0674
M
CE (Cholesteryl esters)
0.0184
0.0196
N
AC (acylcarnitine)
0.0635
0.0438
O
AC (10:0)
0.0121
0.0213
P
OVX vehicle x Vehicle
DPN x Vehicle
OVX DPN x OVX vehicle
Fold-change
Cholesteryl Esters
Individual FA in TG
CE (16:0)
CE (16:1)
CE (18:3)
CE (20:4)
CE (22:5)
CE (22:6)
CE (20:2)
CE (18:1)
CE (18:2)
CE (20:3)
TG (20:3)
TG (20:4)
TG (20:5)
TG (22:4)
TG (22:5)
TG (22:6)
TG (24:5)
TG (10:0)
TG (12:0)
TG (14:0)
TG (14:1)
TG (15:1)
TG (16:0)
TG (16:1)
TG (18:0)
TG (18:2_ox)
TG (17:0)
TG (S/S/S)
TG (S/S/M)
TG (S/M/M)
TG (S/S/P)
TG (S/M/P)
TG (S/P/P)
TG (M/M/M)
TG (M/M/P)
TG (M/P/P)
TG (P/P/P)
TG (ox)
TG (S/S/H)
TG (S/M/H)
TG (S/P/H)
TG (S/H/H)
TG (M/M/H)
TG (M/P/H)
TG (M/H/H)
TG (P/P/H)

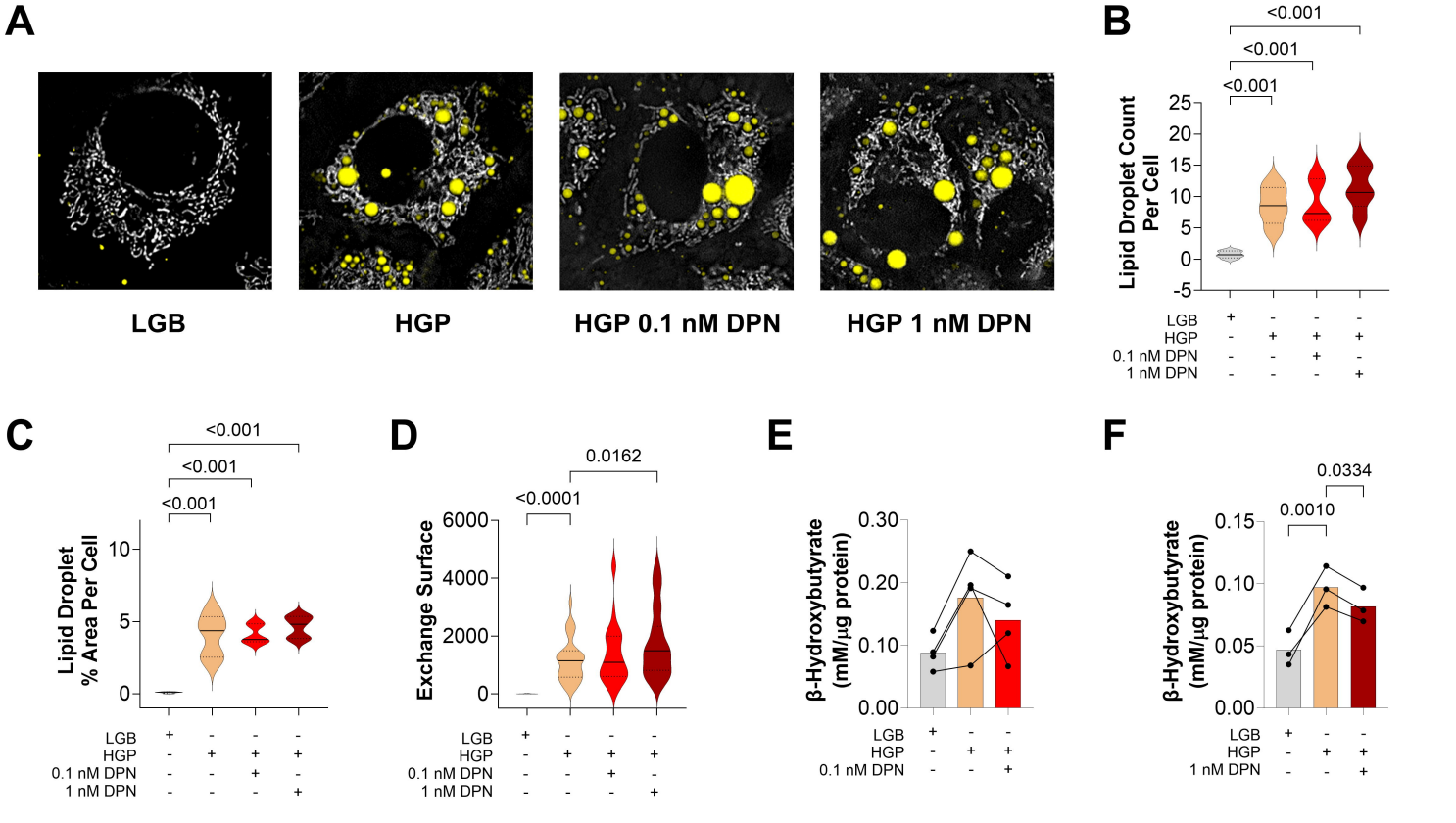
A
LGB
HGP
HGP 0.1 nM DPN
HGP 1 nM DPN
B
Lipid Droplet Count Per Cell
<0.001
<0.001
<0.001
LGB
HGP
0.1 nM DPN
1 nM DPN
C
Lipid Droplet % Area Per Cell
<0.001
<0.001
<0.001
LGB
HGP
0.1 nM DPN
1 nM DPN
D
Exchange Surface
<0.0001
0.0162
LGB
HGP
0.1 nM DPN
1 nM DPN
E
β-Hydroxybutyrate (mM/μg protein)
LGB
HGP
0.1 nM DPN
F
β-Hydroxybutyrate (mM/μg protein)
0.0010
0.0334
LGB
HGP
1 nM DPN

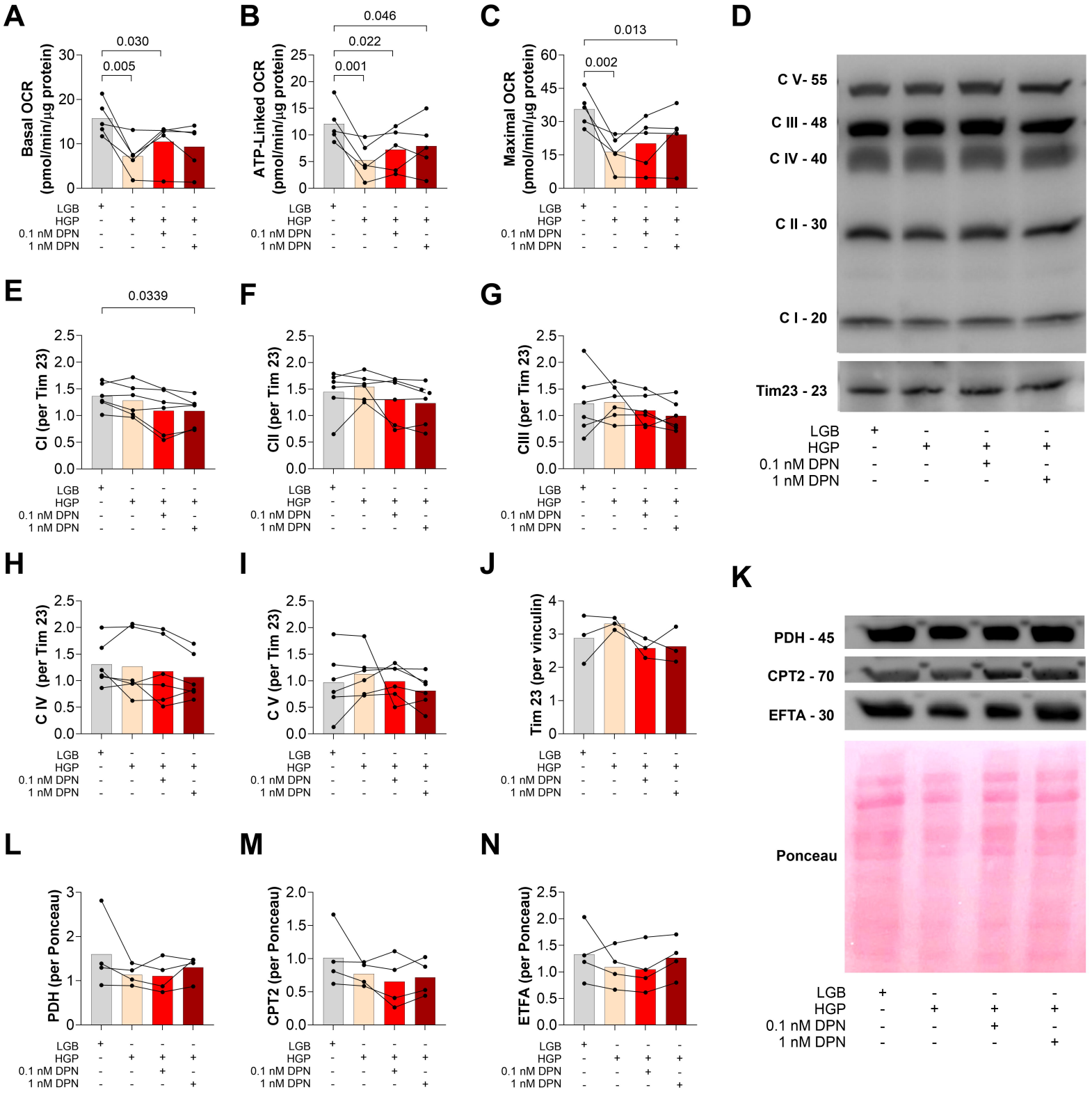
A
Basal OCR (pmol/min/µg protein)
0.030
0.005
B
ATP-Linked OCR (pmol/min/µg protein)
0.046
0.022
0.001
C
Maximal OCR (pmol/min/µg protein)
0.013
0.002
D
C V- 55
C III - 48
C IV - 40
C II - 30
C I - 20
Tim23 - 23
E
CI (per Tim 23)
0.0339
F
CII (per Tim 23)
G
CIII (per Tim 23)
H
C IV (per Tim 23)
I
C V (per Tim 23)
J
Tim 23 (per vinculin)
K
PDH - 45
CPT2 - 70
EFTA - 30
Ponceau
L
PDH (per Ponceau)
M
CPT2 (per Ponceau)
N
ETFA (per Ponceau)
LGB
HGP
0.1 nM DPN
1 nM DPN

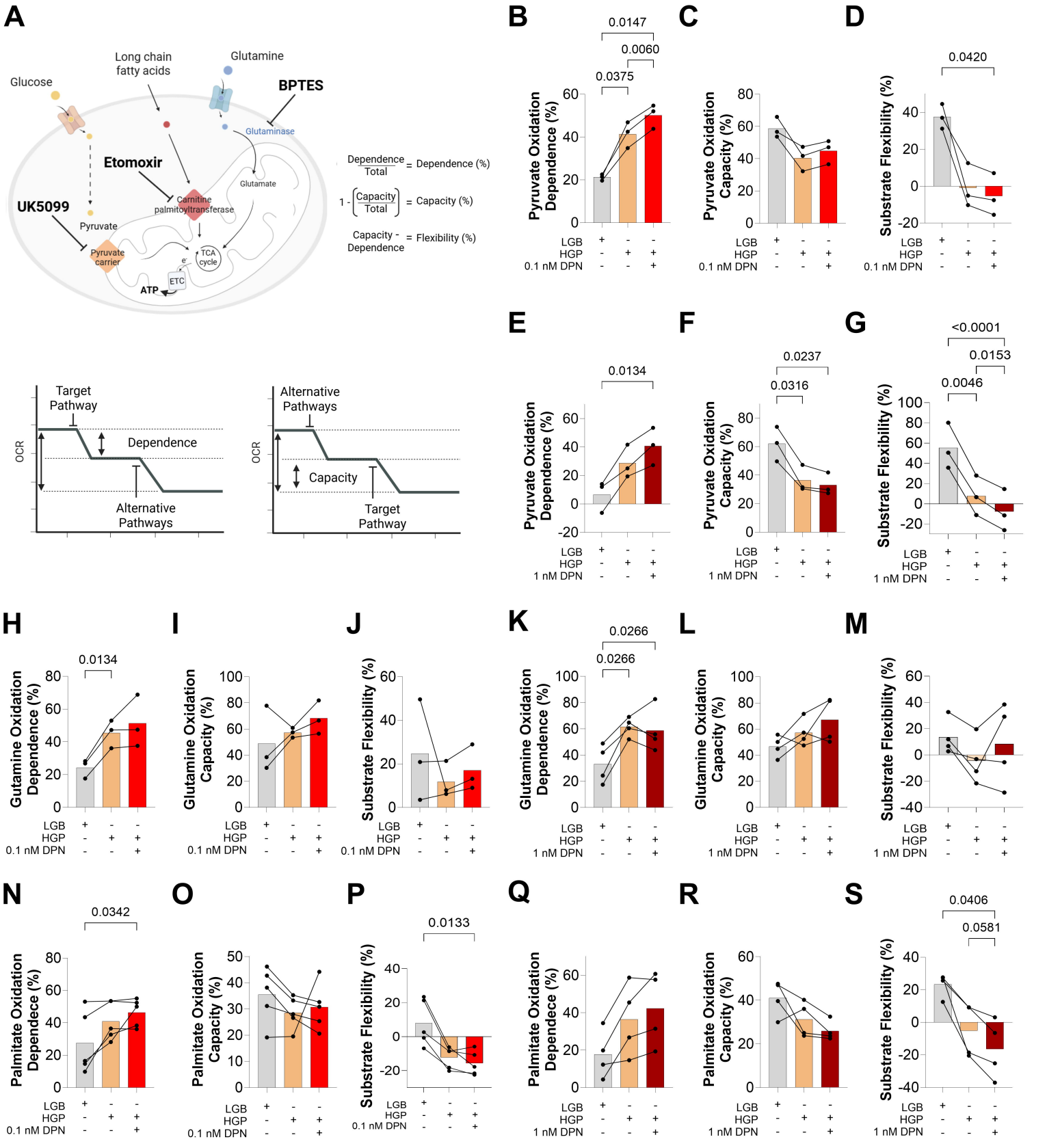
A
Glucose
Long chain fatty acids
Glutamine
BPTES
Glutaminase
Etomoxir
UK5099
Pyruvate
Pyruvate carrier
Carnitine palmitoyltransferase
Glutamate
TCA cycle
ETC
ATP
Dependence / Total = Dependence (%)
1 - (Capacity / Total) = Capacity (%)
Capacity - Dependence = Flexibility (%)
Target Pathway
Dependence
Alternative Pathways
OCR
Alternative Pathways
Capacity
Target Pathway
OCR
B
0.0147
0.0060
0.0375
Pyruvate Oxidation Dependence (%)
LGB
HGP
0.1 nM DPN
C
Pyruvate Oxidation Capacity (%)
D
0.0420
Substrate Flexibility (%)
E
0.0134
Pyruvate Oxidation Dependence (%)
1 nM DPN
F
0.0237
0.0316
Pyruvate Oxidation Capacity (%)
G
<0.0001
0.0153
0.0046
Substrate Flexibility (%)
H
0.0134
Gutamine Oxidation Dependence (%)
I
Glutamine Oxidation Capacity (%)
J
Substrate Flexibility (%)
K
0.0266
0.0266
Glutamine Oxidation Dependence (%)
L
Glutamine Oxidation Capacity (%)
M
Substrate Flexibility (%)
N
0.0342
Palmitate Oxidation Dependece (%)
O
Palmitate Oxidation Capacity (%)
P
0.0133
Substrate Flexibility (%)
Q
Palmitate Oxidation Dependece (%)
R
Palmitate Oxidation Capacity (%)
S
0.0406
0.0581
Substrate Flexibility (%)